Gas Phase UTE MRI of Propane and Propene

Kirill V. Kovtunov[1,2], Alexey S. Romanov[1,2], Oleg G. Salnikov[1,2], Danila A. Barskiy[3], Eduard Y. Chekmenev[3], and Igor V. Koptyug[1,2]

[1]International Tomography Center, Siberian Branch of the Russian Academy of Sciences, Novosibirsk, Russia; [2]Novosibirsk State University, Novosibirsk, Russia; and [3]Department of Radiology, Vanderbilt University Institute of Imaging Science (VUIIS), and Department of Biomedical Engineering, Vanderbilt-Ingram Cancer Center (VICC), Nashville, Tennessee

Corresponding Author:
Kirill V. Kovtunov, PhD
International Tomography Center, SB RAS, 3A Institutskaya St.,
630090, Novosibirsk, Russia;
E-mail: kovtunov@tomo.nsc.ru

Proton magnetic resonance imaging (^{1}H MRI) of gases can potentially enable functional lung imaging to probe gas ventilation and other functions. Here, ^{1}H MR images of hyperpolarized (HP) and thermally polarized propane gas were obtained using ultrashort echo time (UTE) pulse sequence. A 2-dimensional (2D) image of thermally polarized propane gas with $\sim 0.9 \times 0.9$ mm^2 spatial resolution was obtained in <2 seconds, showing that even non-HP hydrocarbon gases can be successfully used for conventional proton magnetic resonance imaging. The experiments were also performed with HP propane gas, and high-resolution multislice FLASH 2D images in $\sim$510 seconds and non-slice-selective 2D UTE MRI images were acquired in $\sim$2 seconds. The UTE approach adopted in this study can be potentially used for medical lung imaging. Furthermore, the possibility of combining UTE with selective suppression of ^{1}H signals from 1 of the 2 gases in a mixture is shown in this MRI study. The latter can be useful for visualizing industrially important processes where several gases may be present, eg, gas–solid catalytic reactions.

INTRODUCTION

Magnetic resonance imaging (MRI) is an established tomographic modality for morphological and functional medical imaging to detect abnormalities in the structure and function of human tissues and organs. However, morphological imaging of the lungs is dominated by such established methods as chest radiography and computed tomography, whereas functional ventilation imaging is conventionally accomplished with the scintigraphy technique (1). In contrast, clinical MRI of human lungs is challenging, because of their low overall density (about one-third of that of muscle tissue) (2) and, consequently, low proton density. Therefore, the signal-to-noise ratio (SNR) that can be achieved in the MRI of the lungs is relatively low. Moreover, the presence of numerous air–tissue interfaces in the lungs leads to significant susceptibility-induced magnetic field gradients, resulting in very short T2* times of the human lung protons [$\sim$1 millisecond in a 1.5 T nuclear magnetic resonance (NMR) scanner (3)]. This further degrades the SNR in the MR images of the lungs. Therefore, the lungs typically appear as dark areas in the conventional proton magnetic resonance (^{1}H MRI) images. The challenge of direct imaging of lung airspace is the main disadvantage for pulmonary applications of MRI.

MRI application for pulmonary imaging is a relatively recent but a rapidly developing field (4). In recent years, significant efforts were made to overcome the limitations of MRI of the lungs (5, 6). In this context, numerous applications have been developed to solve the problem with image artifacts caused by motion. The image acquisition technique during breath-hold or using respiratory gating was developed (7). The problem of susceptibility-induced gradients can be solved by using spin echo radiofrequency (RF) pulse sequences with an extremely short echo time (TE) (8, 9, 10). One of the developed approaches is based on the inhalation of a paramagnetic contrast agent such as gadolinium aerosol (11) or molecular oxygen gas (12, 13) to increase the relaxation rates of tissue protons (14). Nevertheless, a very weak ^{1}H NMR signal from the lung tissue remains the main problem for ^{1}H MRI of the lung. Therefore, the development and utilization of new contrast agents is a very important and promising direction for lung MRI research.

An entirely different approach to the MRI of void spaces in a broad range of materials and structures in general, and lung MRI in particular, is the direct imaging of a suitable gas filling those voids. In particular, perfluorinated gases such as SF_6 and C_nF_{2n+2} (n = 1–3) (15) are a potentially good alternative for pulmonary MRI (16), because the ^{19}F isotope has a high gyromagnetic ratio and 100% natural abundance. Utilization of perfluorinated gases allows for a high contrast with the surrounding tissue because of the lack of a background signal. However, the gas-phase MRI of the lung faces the same motion and susceptibility problems as the ^{1}H MRI of the lung, whereas the spin density problem for gases is the severest, which results in a relatively low spatial and temporal resolution (17, 18). For

[19]F MRI of gases, a low SNR can be partially compensated by the use of short repetition time (TR), as the gases' T1 is in the millisecond range. The problem of low sensitivity is also addressed by using hyperpolarized (HP) nonproton contrast gas agents such as [3]He or [129]Xe (19, 20, 21). However, in the case of He, Xe, or fluorinated gases, multinuclear RF coil and transmitter/receiver are required, whereas standard clinical MRI scanners lack these capabilities. In addition, production of HP noble gases is relatively expensive and requires sophisticated *hyperpolarizer* instrumentation (22-25). Nevertheless, the potential advantages of gas MRI for pulmonary imaging, such as lack of ionizing radiation, and the potential applicability for diagnostics and monitoring response to therapy of various diseases, for example, chronic obstructive pulmonary disease, emphysema, asthma, and cystic fibrosis, make further efforts in this field worthwhile.

[1]H MRI of hydrocarbon gases may be of interest for a range of applications, including imaging of materials, chemical reactors, and lung MRI. One of the promising candidate gases is propane, which is widely used in the food industry and in cosmetics. It is a nontoxic asphyxiant gas, and it was reported that brief inhalation exposures to 10 000 ppm of propane causes no toxicity in humans (26). Moreover, propane in concentrations of 250, 500, or 1000 ppm for periods of 1 minute to 8 hours did not produce any unfavorable physiological effects in humans. Repetitive exposures to propane also did not cause any measurable physiological effects (27). The major advantage of using hydrocarbon gases in MRI is that the ^{1}H transmit/receive capability can be implemented on any MRI system.

However, ^{1}H MRI of gases is an underdeveloped research area, largely because of the challenges of gas imaging discussed above. Nevertheless, the feasibility of ^{1}H MRI of hydrocarbon gases such as acetylene, propane, and butane at atmospheric pressures was shown about 15 years ago, with 2-dimensional (2D) images of flowing and static gas and flow velocity maps in pipes and multichannel monolith structures detected using a spin-echo pulse sequence (28, 29). In addition to the low spin density of gases, the rapid diffusion of gases in applied magnetic field gradients further reduces the detected signal for pulse sequences with relatively long TE. Therefore, image acquisition times were fairly long (20–40 minutes for the each 2D image), which may significantly limit gas MRI applications (30). Thus, imaging of gases may considerably benefit from the development of pulse sequences with ultrashort TE, as shown recently in the spectroscopic imaging study of ethylene to ethane conversion in a model catalytic reactor (31).

Another strategy for improving sensitivity in gas MRI is the use of HP gases, as mentioned above, for [3]He and [129]Xe. Hyperpolarization techniques are also available for producing hydrocarbon gases. Parahydrogen-induced polarization (PHIP) (32-34) is a unique technique for producing gases with HP ^{1}H nuclei by heterogeneous (35) or biphasic (36) pairwise addition of parahydrogen to a suitable unsaturated gaseous substrate (eg, hydrogenation of propene to propane). Heterogeneous hydrogenation is the most robust approach, because the catalyst can be recycled many times and the produced HP gas is free from the catalyst. In addition, the HP gas can be continuously produced, and thus, can be continuously renewed in the voids of an object

under study to maintain high signal intensity for the duration of image acquisition, as demonstrated in 2D (37, 38) and 3-dimensional (3D) imaging of various model objects with submillimeter spatial resolution (39). Moreover, the use of remote detection allows to image micro-channels with appropriate resolution by using the HP gas (40, 41). However, despite favorable properties of HP propane, such as high polarization levels and continuous production, a significant fundamental challenge for the use of HP propane is its relatively short T1 in high magnetic fields (<1 second at standard temperature and pressure) (42). This becomes a major problem in the studies where continuous HP gas replenishment is not feasible, for instance, in lung imaging. One promising option is the use of long-lived spin states that can be used to store polarization for time periods significantly exceeding T1 (43, 44). Recently, a relatively long hyperpolarization lifetime T_{LLSS} was achieved for HP propane-d_6 (∼6.0 seconds) (45) and for HP propane (4.7 ± 0.5 s) (46) in low magnetic fields. Thus, to make HP propane that is produced via propene hydrogenation with parahydrogen over different supported metals (47, 48) a promising candidate for lung imaging and other applications, implementation of rapid image acquisition schemes with imaging times of the order of 1–2 seconds or less is required.

Motivated by the aforementioned technical and biomedical challenges, the present work focused on the development of strategies for ^{1}H MRI visualization of both HP and thermally polarized propane gas for high-resolution MRI applications.

METHODOLOGY

NMR and MRI experiments were performed on an Avance™ III 400 MHz NMR spectrometer (Bruker) equipped with microimaging accessories. The experiments were conducted with a commercial 15-mm ID RF coil (Bruker) using ^{1}H channel. In all MRI experiments, shim values optimized on a sample comprising propane gas in a standard 10-mm NMR tube (Wilmad) were used, resulting in line width at half maximum of ∼5 Hz. MR images were obtained using ParaVision (Bruker) software. Ultrashort echo time (UTE) pulse sequence was used with a total acquisition time of 2 seconds for MRI imaging of propane and total acquisition time of 8 seconds, and a spectral width of 100 kHz for propane and propene. TR was 20 milliseconds and TE was 0.226 milliseconds. The k-space in the UTE sequence is scanned along radial trajectories, and the number of projections was equal to 100 and 400 for 32 × 32 and 128 × 128 image matrix sizes, respectively. The image resolution of 0.94 × 0.94 mm² (32 × 32 matrix) was used for experiments with HP propane and 0.39 × 0.39 mm² (matrix 128 × 128) for experiments with selective NMR signal suppression. The pulse angle was equal to 25° for a FLASH sequence and 15° for all experiments with the UTE sequence. All MRI experiments with thermally polarized propane were conducted using a single 15-mm NMR tube. For MRI experiments with selective signal suppression, a 10-mm NMR tube filled with propene was placed inside a 15-mm tube containing propane. For HP propane production, a mixture containing 50% parahydrogen and 50% orthohydrogen (referred to as pH_2 below) was first produced by passing normal hydrogen through the ortho-para conversion catalyst (FeO(OH)) kept at 77 K. The propane:pH_2 (1:4) gas mixture was
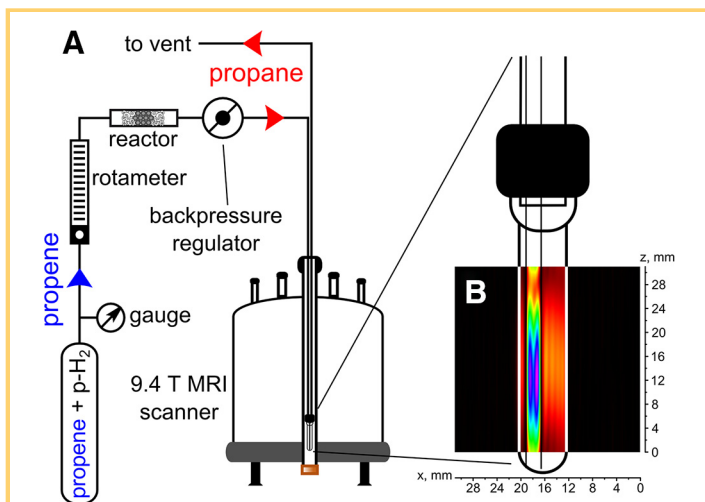
Figure 1. The schematic representation of the experimental setup for producing parahydrogen-induced polarization (PHIP) hyperpolarized (HP) propane via heterogeneous pairwise hydrogenation of propene with parahydrogen (A). An overlay of hydrogen 1 (^{1}H) magnetic resonance imaging (^{1}H MRI) FLASH image of hyperpolarized (HP) propane flowing into the 10-mm nuclear magnetic resonance (NMR) tube via 1/16″ OD Teflon capillary (B). The field of view (FOV) was 3.1 × 3.1 cm with 256 × 32 matrix size, and the total acquisition time was ~510 seconds. Note that the NMR tube is schematically shown, and its length does not correlate with the actual scale of the 2-dimensional (2D) magnetic resonance (MR) image.

passed through Rh/TiO_2 heterogeneous catalyst held at 250°C [ALTADENA experimental conditions (49)]. The flow rate of HP propane/pH_2 mixture was maintained at ~20 mL/s for the duration of imaging acquisition. HP propane was flowing through the 1/16″ OD Teflon capillary extended to the bottom of a standard 10-mm NMR tube. The modified FLASH pulse sequence (50) was also used for image acquisition. The modification by using the selective saturation of the unwanted resonance of CH_2 propane group immediately before application of a FLASH sequence was applied. Thus, the problem of cancellation of the opposite CH_3 ALTADENA NMR signal of propane with negative CH_2 ALTADENA propane signal was solved. The total imaging time to acquire 4 slices with 256 × 32 matrix size was ~8.5 minutes. The schematic representation of the experimental setup and the corresponding overlay of FLASH MRI image are shown in Figure 1.

RESULTS AND DISCUSSION
FLASH MRI
HP propane was produced via heterogeneous hydrogenation of propene with pH_2 over Rh/TiO_2 catalyst (31). The reaction scheme for HP propane formation is shown in Figure 2A. The initial experiments on propane ^{1}H MRI (41) were performed

using the same type of setup and a relatively time-consuming 2D image FLASH acquisition of ~510 seconds. Here, we used conventional FLASH pulse sequence to acquire four 2D slices with the spatial resolution of 0.1 × 0.8 mm^2 with the same total acquisition time. Therefore, using FLASH may be preferable for multislice 2D gas MRI. Note that significant signal enhancement obtained via PHIP is crucial for ^{1}H FLASH MRI of the gaseous phase. Signal enhancement of up to 30 times for HP propane versus thermally polarized propane (Figure 2B) allows one to detect images with spatial resolution that is sufficient to detect flowing HP gas in a 1/16″ OD Teflon capillary (Figure 2C). The 2 bright spots in the capillary are the artifacts of the FLASH pulse sequence and show the position of the main flow inside the capillary. Note that the same experiment with thermally polarized propane did not produce any meaningful image because of the insufficient SNR (data not shown). However, as discussed above, the visualization of HP gas with short T1 faces additional difficulties for applications where the imaged volume cannot be continuously replenished with the HP gas, considerably limiting the possibilities for widespread biomedical utilization of the gas-phase lung MRI. Therefore, despite the obvious success of obtaining high-resolution FLASH images above, this approach will face considerable challenges for clinical translation. Therefore, the development of ultrafast imaging approaches for imaging of nonflowing gas (ie, simulating the conditions of inhaled gas in the in vivo studies) is much desired for potential MRI of the lungs.

Recently, ultrafast MRI pulse sequences based on radial acquisition of k-space data were used for lung MRI owing to the fact that they can reduce TE down to 100 μs. Such short TE allows one to minimize the signal decay caused by the short transverse relaxation time (T2*) of the lung tissue (8, 51). Moreover, it was shown that the short TE makes it possible to quantitatively verify regional T2* values and morphological changes in mice by comparing normal lungs and lungs with pulmonary emphysema (52, 53). Furthermore, such ultrashort TE sequences could arguably be beneficial for contrast agents with short T2 and T1 as well, which was the next step in our investigation.

UTE Studies
First, conventional UTE pulse sequence (as implemented in Bruker ParaVision) was used for ^{1}H MR imaging of static propane gas at thermal polarization levels. It was shown that UTE can indeed visualize a hydrocarbon gas with good spatial resolution (Figure 3A). UTE allowed for a very short TE of 200 μs in our gas experiments, which is approximately one order of magnitude improvement compared with the previous studies of continuously flowing gas at high magnetic fields (38) and ~35-fold improvement compared with the low-field MRI studies of stopped propane gas (35). Therefore, the negative impact of fast diffusion on the signal loss during gradient switching is considerably reduced. By decreasing the matrix size, we were able to reduce the image acquisition time to 2 seconds.

In the next experiment, HP propane gas produced by heterogeneous hydrogenation of propene over Rh/TiO_2 catalyst with pH_2 was imaged in a similar way to the thermally polarized gas above, except that HP propane was flowing during imaging. The signal intensity of HP propane is only 2 times higher than
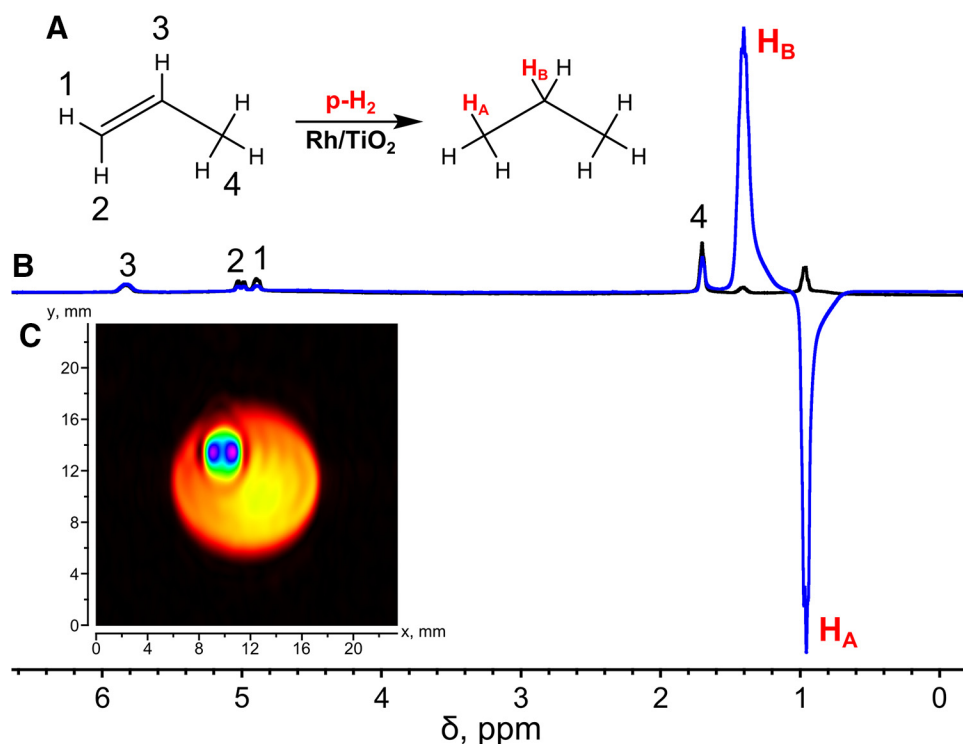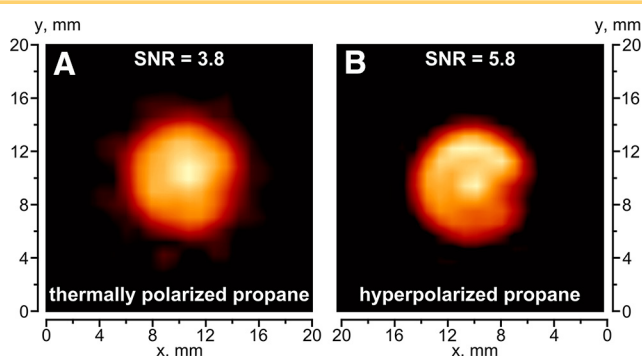
Figure 2. Heterogeneous hydrogenation of propene to propane with pH₂ over Rh/TiO₂ catalyst with partial preservation of spin order of parahydrogen in the final HP product (A). ¹H NMR spectra of HP propane (blue) and thermally polarized propane (black) obtained in heterogeneous hydrogenation of propene with parahydrogen; the signal enhancement was ∼30-fold (B). ¹H MRI of HP propane flowing through a 1/16″ OD Teflon capillary inside a 10-mm NMR tube obtained with a FLASH pulse sequence (C). The FOV was 3.1 × 2.5 cm with 256 × 32 matrix size, and the total acquisition time was ∼510 seconds with slice thickness of ∼0.7 cm. The signal intensity color scale ranges from black (zero) to blue (maximum).

that of thermally polarized propane (Figure 3, A and B). Simultaneously, comparison of the corresponding ¹H NMR spectra acquired under the same conditions gave the signal enhan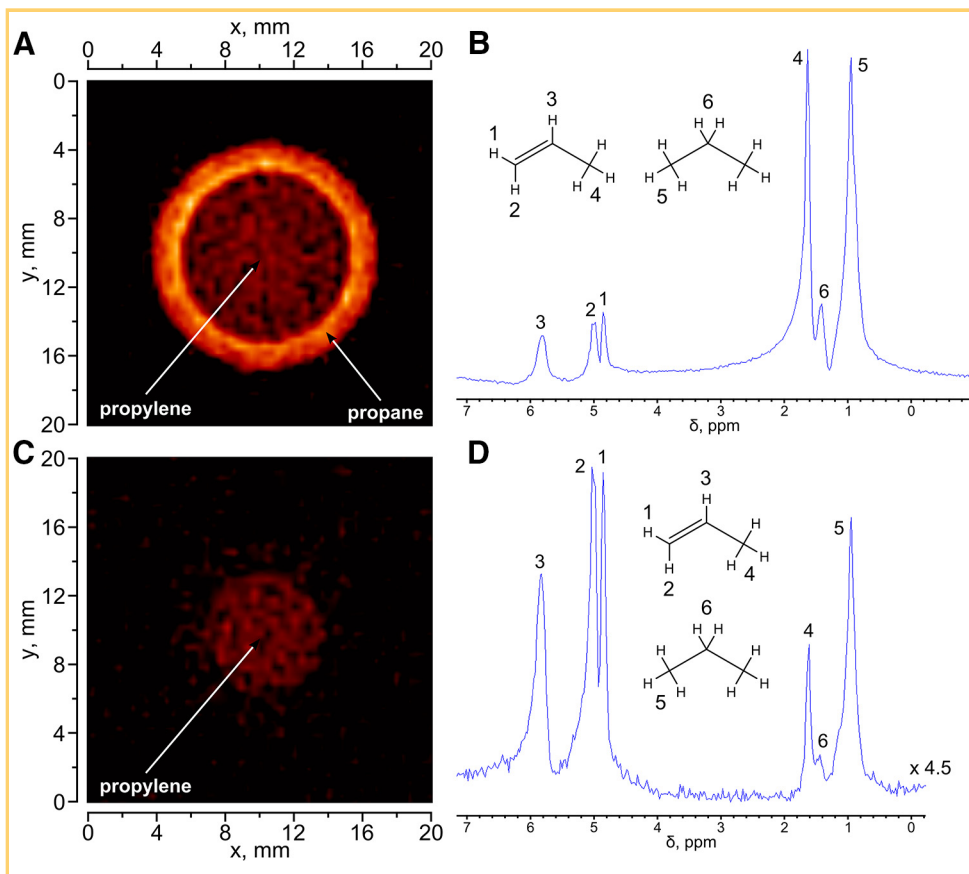cement factor of ∼10. This apparent discrepancy in signal enhancements between ¹H MR images and ¹H NMR spectra can be explained as an intrinsic feature of the UTE pulse sequence and, to a greater extent, by the nature of acquisition under stopped and flowing gas conditions. More importantly, we believe that this is the first report of the feasibility to acquire gas-phase ¹H MR image of a hydrocarbon gas in time suitable for image acquisition of nonflowing gas on a single patient breath-hold (∼2 seconds). Although some additional parameters can be optimized in the future and the imaging can be extended to either 3D or a multislice 2D version, the use of short TE and UTE sequences paves the way for future biomedical and other uses of thermally polarized gases, as well as HP gases. Arguably, the acquisition time needs to be further shortened for HP imaging application for contrast agents with T1 <1 second. Alternatively, the advances in development and design of long-lived spin states can be potentially used to increase the relaxation time of HP hydrocarbons at high magnetic fields (36, 44, 54).

Figure 3. MR images of 15-mm NMR tube filled with thermally polarized propane (A) and PHIP HP propane (the same experimental setup as for Figure 1) (B). The FOV was 3 × 3 cm with 32 × 32 matrix size, the total acquisition time was ∼2 seconds, and the slice thickness in the z direction was 10 mm.

MRI of Gases with Chemical Selectivity

In some applications, it would be desirable to combine rapid gas imaging with chemical (spectroscopic) selectivity. For instance, binary gas mixtures can be imaged using selective signal suppression of one of the gases, which could be potentially useful for chemical selectivity for future *operando* imaging studies of catalytic reactors. Nowadays, MRI of the lung with HP noble

Figure 4. ^{1}H MR image (A) and corresponding ^{1}H NMR spectrum of a sample comprising a 10-mm NMR tube with propylene placed inside a 15-mm tube with propane (B). ^{1}H MR image (C) and corresponding ^{1}H NMR spectrum (D) of the same phantom with application of selective suppression pulse for propane NMR signals. The FOV for both images was 5 × 5 cm with 128 × 128 matrix size and 10-mm slice thickness along the z axis; the total acquisition time was ~8 seconds. The ^{1}H NMR spectrum was obtained using the same ultrashort echo time (UTE) pulse sequence as that for ^{1}H MRI but with the gradients switched off and the spectral bandwidth appropriately reduced.

gases and conventional ^{1}H MRI can be simultaneously performed within the same inhalation (55). Such an approach has many potential applications, allowing side-by-side quantitative analysis of early signs of impaired lung function from HP gases and anatomic signs of disease from the ^{1}H MR images (56).

Therefore, we used the approach presented above to demonstrate the feasibility of selective suppression of NMR signals in a specific region of an NMR spectrum during the gas-phase MRI. To this end, we used a model sample comprising a 10-mm NMR tube with 1 atm of propylene placed inside a 15-mm NMR tube with 1 atm of propane (Figure 4A).

The results show that the conventional UTE pulse sequence allows one to simultaneously visualize propane and propylene (Figure 4A) without significant image artifacts. This is possible owing to a very large spectral width used during signal acquisition (100 kHz), corresponding to the image encoding with ~3.125 kHz/pixel, which exceeds the chemical shift dispersion of ~2.2 kHz at 9.4 T (Figure 4). However, the ^{1}H MRI signal of propylene is somewhat less intense, and this fact may be explained by different relaxation times of propane and propylene and fewer protons in the propylene molecule. The acquired ^{1}H NMR spectrum (Figure 4B) shows the presence of propane and propylene in the same phantom and their relative quantities. For the next set of experiments, selective suppression pulse for CH_3 and CH_2 groups of propane was added to the UTE sequence before image detection. This significantly changes the ^{1}H NMR spectrum (Figure 4D), and the NMR line intensities of the CH_3 and CH_2 groups of propane show an ~10-fold decrease. This also reduces the signal of the CH_3 group of propylene, so that the major signals remaining in the ^{1}H NMR spectrum are those of

the CH and CH_2 groups of propylene. Their ^{1}H signal is sufficient to visualize propylene by ^{1}H MRI (Figure 4C). Such observations have not been previously reported.

CONCLUSIONS

^{1}H MRI of continuously flowing HP propane gas produced by heterogeneous hydrogenation of propylene with parahydrogen (ALTADENA regime) was performed using 2 different MRI pulse sequences. Compared with the FLASH sequence, the use of UTE MRI significantly decreases the total imaging time down to the regime sufficient for MRI of a patient within a single breath-hold in future clinical translation. Further reduction in the acquisition time via compressed sensing and further reduction in TR may render 3D UTE gas-phase imaging possible on a single breath-hold.

It was found that a conventional UTE pulse sequence allows one to obtain a 2D image of thermally polarized gas with ~0.9 × 0.9 mm^2 spatial resolution in ~2 seconds, which is much faster compared with the FLASH acquisition even if the latter is optimized to reduce the imaging time. Importantly, it was shown for the first time that the UTE pulse sequence is very efficient for ^{1}H MRI of a thermally polarized gas. The imaging of HP gas with UTE provided additional signal enhancement gains - a major advantage in the context of biomedical and industrial applications. Note that in the case of the HP gas, a single image can be acquired if the gas is not flowing, whereas for repetitive imaging, the HP gas should be imaged under flow conditions. In contrast, thermally polarized gas and UTE pulse sequence allow one to detect multiple images even at 1 inhalation. Moreover, the ability of selective suppression of proton signals enables MRI

imaging with chemical selectivity in the gas phase without significant sacrifice in the total imaging speed. The obtained results are transitional steps for converting the described approach to medical lung imaging, and the UTE pulse sequence appears to be the main candidate for in vivo imaging of lung with a nontoxic hydrocarbon gas.

REFERENCES

1. Bajc M, Neilly JB, Miniati M, Schuemichen C, Meignan M, Jonson B, EANM Committee. EANM guidelines for ventilation/perfusion scintigraphy: Part 1. Pulmonary imaging with ventilation/perfusion single photon emission tomography. Eur J Nucl Med Mol Imaging. 2009;36(8):1356–1370.

2. Hatabu H, Alsop DC, Listerud J, Bonnet M, Gefter WB. T2* and proton density measurement of normal human lung parenchyma using submillisecond echo time gradient echo magnetic resonance imaging. Eur J Radiol. 1999; 29(3):245–248.

3. Stock KW, Chen Q, Hatabu H, Edelman RR. Magnetic resonance T2* measurements of the normal human lung in vivo with ultra-short echo times. Magn Reson Imaging. 1999;17(7):997–1000.

4. Conradi MS, Saam BT, Yablonskiy DA, Woods JC. Hyperpolarized He-3 and perfluorocarbon gas diffusion MRI of lungs. Prog Nucl Mag Res Sp. 2006;48(1): 63–83.

5. Ohno Y, Oshio K, Uematsu H, Nakatsu M, Gefter WB, Hatabu H. Single-shot half-Fourier RARE sequence with ultra-short inter-echo spacing for lung imaging. J Magn Reson Imaging. 2004;20(2):336–339.

6. Eibel R, Herzog P, Dietrich O, Rieger CT, Ostermann H, Reiser MF, Schoenberg SO. Pulmonary abnormalities in immunocompromised patients: comparative detection with parallel acquisition MR imaging and thin-section helical CT. Radiology. 2006;241(3):880–891.

7. Larson AC, Kellman P, Arai A, Hirsch GA, McVeigh E, Li D, Simonetti OP. Preliminary investigation of respiratory self-gating for free-breathing segmented cine MRI. Magn Reson Med. 2005;53(1):159–168.

8. Johnson KM, Fain SB, Schiebler ML, Nagle S. Optimized 3D ultrashort echo time pulmonary MRI. Magn Reson Med. 2013;70(5):1241–1250.

9. Togao O, Ohno Y, Dimitrov I, Hsia CC, Takahashi M. Ventilation/perfusion imaging of the lung using ultra-short echo time (UTE) MRI in an animal model of pulmonary embolism. J Magn Reson Imaging. 2011;34(3):539–546.

10. Ohno Y, Koyama H, Yoshikawa T, Matsumoto K, Takahashi M, Van Cauteren M, Sugimura K. T2* measurements of 3-T MRI with ultrashort TEs: capabilities of pulmonary function assessment and clinical stage classification in smokers. AJR Am J Roentgenol. 2011;197(2):W279–W285.

11. Sood BG, Shen Y, Latif Z, Chen X, Sharp J, Neelavalli J, Joshi A, Slovis TL, Haacke EM. Aerosol delivery in ventilated newborn pigs: an MRI evaluation. Pediatr Res. 2008;64(2):159–164.

12. Bauman G, Eichinger M. Ventilation and perfusion magnetic resonance imaging of the lung. Pol J Radiol. 2012;77(1):37–46.

13. Ohno Y, Hatabu H, Takenaka D, Van Cauteren M, Fujii M, Sugimura K. Dynamic oxygen-enhanced MRI reflects diffusing capacity of the lung. Magn Reson Med. 2002;47(6):1139–1144.

14. Mosbah K, Ruiz-Cabello J, Berthezène Y, Crémillieux Y. Aerosols and gaseous contrast agents for magnetic resonance imaging of the lung. Contrast Media Mol Imaging. 2008;3(5):173–190.

15. Ruiz-Cabello J, Barnett BP, Bottomley PA, Bulte JWM. Fluorine (19F) MRS and MRI in biomedicine. NMR Biomed. 2011;24(2):114–129.

16. Jacob RE, Chang YV, Choong CK, Bierhals A, Hu DZ, Zheng J, Yablonskiy DA, Woods JC, Gierada DS, Conradi MS. 19F MR imaging of ventilation and diffusion in excised lungs. Magn Reson Med. 2005;54(3):577–585.

17. Kuethe DO, Caprihan A, Gach HM, Lowe IJ, Fukushima E. Imaging obstructed ventilation with NMR using inert fluorinated gases. J Appl Physiol (1985). 2000; 88(6):2279–2286.

18. Kuethe DO, Caprihan A, Fukushima E, Waggoner RA. Imaging lungs using inert fluorinated gases. Magn Reson Med. 1998;39(1):85–88.

19. Lilburn DM, Pavlovskaya GE, Meersmann T. Perspectives of hyperpolarized noble gas MRI beyond ³He. J Magn Reson. 2013;229:173–186.

20. Nikolaou P, Goodson BM, Chekmenev EY. NMR hyperpolarization techniques for biomedicine. Chem Eur J. 2015;21:3156–3166.

21. Kirby M, Ouriadov A, Svenningsen S, Owrangi A, Wheatley A, Etemad-Rezai R, Santyr GE, McCormack DG, Parraga G. Hyperpolarized ³He and ¹²⁹Xe magnetic resonance imaging apparent diffusion coefficients: physiological relevance in older never- and ex-smokers. Physiol Rep. 2014;2(3). pii: e12068.

22. Goodson BM. Nuclear magnetic resonance of laser-polarized noble gases in molecules, materials, and organisms. J Magn Reson. 2002;155(2):157–216.

23. Capozzi A, Roussel C, Comment A, Hyacinthe JN. Optimal glass-forming solvent brings sublimation dynamic nuclear polarization to ¹²⁹Xe hyperpolarization biomedical imaging standards. J Phys Chem C. 2015;119(9):5020–5025.

24. Nikolaou P, Coffey AM, Walkup LL, Gust BM, Whiting N, Newton H, Barcus S, Muradyan I, Dabaghyan M, Moroz GD, Rosen M, Patz S, Barlow MJ, Chekmenev EY, Goodson BM. Near-unity nuclear polarization with an open-source 129Xe hyperpolarizer for NMR and MRI. Proc Natl Acad Sci U S A. 2013; 110(35):14150–14155.

25. Mugler JP, Altes TA. Hyperpolarized ¹²⁹Xe MRI of the human lung. J Magn Reson Imaging. 2013;37(2):313–331.

26. Braker W, Mossman AL. Matheson Gas Data Book. 6th ed. Secaucus, NJ: Matheson Gas Products-USA; 2010.

27. Stewart RD, Newton PE, Baretta ED, Herrmann AA, Forster HV, Soto RJ. Physiological response to aerosol propellants. Environ Health Perspect. 1978;26: 275–285.

28. Koptyug IV, Altobelli SA, Fukushima E, Matveev AV, Sagdeev RZ. Thermally polarized (1)H NMR microimaging studies of liquid and gas flow in monolithic catalysts. J Magn Reson. 2000;147(1):36–42.

29. Koptyug IV, Matveev AV, Altobelli SA. NMR studies of hydrocarbon gas flow and dispersion. Appl Magn Reson. 2002;22:187–200.

30. Newling B. Gas flow measurements by NMR. Prog Nucl Magn Reson Spectrosc. 2008;52:31–48.

31. Ulpts J, Dreher W, Klink M, Thoming J. NMR imaging of gas phase hydrogenation in a packed bed flow reactor. Applied Catalysis A: General. 2015;502: 340–349.

32. Bowers CR, Weitekamp DP. Transformation of symmetrization order to nuclear-spin magnetization by chemical reaction and nuclear magnetic resonance. Phys Rev Lett. 1986; 57(21):2645–2648;

33. Natterer J, Bargon J. Parahydrogen induced polarization. Prog Nucl Magn Reson Spectrosc. 1997;31(4):293–315.

34. Bowers CR, Weitekamp DP. Parahydrogen and synthesis allow dramatically enhanced nuclear alignment. J Am Chem Soc. 1987;109(18):5541–5542.

35. Kovtunov KV, Beck IE, Bukhtiyarov VI, Koptyug IV. Observation of parahydrogen-induced polarization in heterogeneous hydrogenation on supported metal catalysts. Angew Chem Int Ed Engl. 2008;47(8):1492–1495.

36. Kovtunov KV, Zhivonitko VV, Skovpin IV, Barskiy DA, Salnikov OG, Koptyug IV. Toward continuous production of catalyst-free hyperpolarized fluids based on biphasic and heterogeneous hydrogenations with parahydrogen. J Phys Chem C. 2013;117(44):22887–22893.

37. Bouchard LS, Kovtunov KV, Burt SR, Anwar MS, Koptyug IV, Sagdeev RZ, Pines A. Parahydrogen-enhanced hyperpolarized gas-phase magnetic resonance imaging. Angew Chem Int Ed Engl. 2007;46(22):4064–4068.

38. Bouchard LS, Burt SR, Anwar MS, Kovtunov KV, Koptyug IV, Pines A. NMR imaging of catalytic hydrogenation in microreactors with the use of para-hydrogen. Science. 2008;319(5862):442–445.

39. Kovtunov KV, Barskiy DA, Coffey AM, Truong ML, Salnikov OG, Khudorozhkov AK, Inozemtseva EA, Prosvirin IP, Bukhtiyarov VI, Waddell KW, Chekmenev EY, Koptyug IV. High-resolution 3D proton MRI of hyperpolarized gas enabled by parahydrogen and Rh/TiO2 heterogeneous catalyst. Chemistry - A European Journal. 2014;20:11636–11639.

40. Zhivonitko VV, Telkki VV, Koptyug IV. Characterization of microfluidic gas reactors using remote-detection MRI and parahydrogen-induced polarization. Angew Chem Int Ed Engl. 2012;51(32):8054–8058.

41. Telkki VV, Zhivonitko VV, Ahola S, Kovtunov KV, Jokisaari J, Koptyug IV. Microfluidic gas-flow imaging utilizing parahydrogen-induced polarization and remote-detection NMR. Angew Chem Int Ed. 2010;49(45):8363–8366.

42. Barskiy DA, Salnikov OG, Kovtunov KV, Koptyug IV. NMR signal enhancement for hyperpolarized fluids continuously generated in hydrogenation reactions with parahydrogen. J Phys Chem A. 2015;119(6):996–1006.

43. Warren WS, Jenista E, Branca RT, Chen X. Increasing hyperpolarized spin lifetimes through true singlet eigenstates. Science. 2009;323(5922):1711–1714.

44. Carravetta M, Levitt MH. Long-lived nuclear spin states in high-field solution NMR. J Am Chem Soc. 2004;126(20):6228–6229.

45. Kovtunov KV, Truong ML, Barskiy DA, Salnikov OG, Bukhtiyarov VI, Coffey AM, Waddell KW, Koptyug IV, Chekmenev EY. Propane-d6 heterogeneously hyperpolarized by parahydrogen. J Phys Chem C. 2014;118(48):28234–28243.

46. Kovtunov KV, Truong ML, Barskiy DA, Koptyug IV, Waddell KW, Chekmenev EY. Long-lived spin states for low-field hyperpolarized gas MRI. Chemistry - A European Journal. 2014;20(45):14629–14632.

47. Zhao EW, Zheng H, Ludden K, Xin Y, Hagelin-Weaver HE, Bowers CR. Strong metal–support interactions enhance the pairwise selectivity of parahydrogen addition over Ir/TiO2. ACS Catal. 2016;6(2):974–978.

48. Salnikov OG, Kovtunov KV, Barskiy DA, Bukhtiyarov VI, Kaptein R, Koptyug IV. Kinetic study of propylene hydrogenation over Pt/Al2O3 by parahydrogen-induced polarization. Appl Magn Reson. 2013;44(1):279–288.

49. Pravica MG, Weitekamp DP. Net NMR alignment by adiabatic transport of para-hydrogen addition products to high magnetic field. Chem Phys Lett. 1988; 145(4):255–258.

50. Haase A, Frahm J, Matthaei D, Hanicke W, Merboldt KD. FLASH imaging: rapid NMR imaging using low flip angle pulses. J Magn Reson. 2011;213(2):533–541.

51. Gewalt SL, Glover GH, Hedlund LW, Cofer GP, MacFall JR, Johnson GA. MR microscopy of the rat lung using projection reconstruction. Magn Reson Med. 1993;29:99–108.

52. Togao O, Tsuji R, Ohno Y, Dimitrov I, Takahashi M. Ultrashort echo time (UTE) MRI of the lung: assessment of tissue density in the lung parenchyma. Magn Reson Med. 2010;64(5):1491–1498.

53. Takahashi M, Togao O, Obara M, Cauteren M, Ohno Y, Doi S, Kuro-o M, Malloy C, Hsia CC, Dimitrov I. Ultrashort echo time (UTE) MR imaging of the lung: comparison between normal and emphysematous lungs in mutant mice. J Magn Reson Imaging. 2010;32(2):326–333.

54. Pileio G, Carravetta M, Hughes E, Levitt MH. The long-lived nuclear singlet state of 15N-nitrous oxide in solution. J Am Chem Soc. 2008;130(38):12582–12583.

55. Horn FC, Tahir BA, Stewart NJ, Collier GJ, Norquay G, Leung G, Ireland RH, Parra-Robles J, Marshall H, Wild JM. Lung ventilation volumetry with same-breath acquisition of hyperpolarized gas and proton MRI. NMR Biomed. 2014;27(12): 1461–1467.

56. Wild JM, Marshall H, Xu X, Norquay G, Parnell SR, Clemence M, Griffiths PD, Parra-Robles J. Simultaneous imaging of lung structure and function with triple-nuclear hybrid MR imaging. Radiology. 2013;267(1):251–255.